CD20+ natural killer cells are polyfunctional, memory-like cells that are enriched in inflammatory disorders

Özgür Albayrak, Ergün Tiryaki, Nazan Akkaya, Ali Burak Kzlrmak, Tansu Doran, Gökçe Gökmenolu, Muhammed Yüksel, Bürge Ulukan, Mina Üzülmez, Il Baytekin, Önder Kemal Soylu, Güne Esendal, Ingrid Meinl, Mesrure Köseolu, Burcu Yüksel, Suat Erus, Çidem Arkan, Seçil Vural, Müjdat Zeybel, Aysun Soysal, Edgar Meinl, Atay Vural

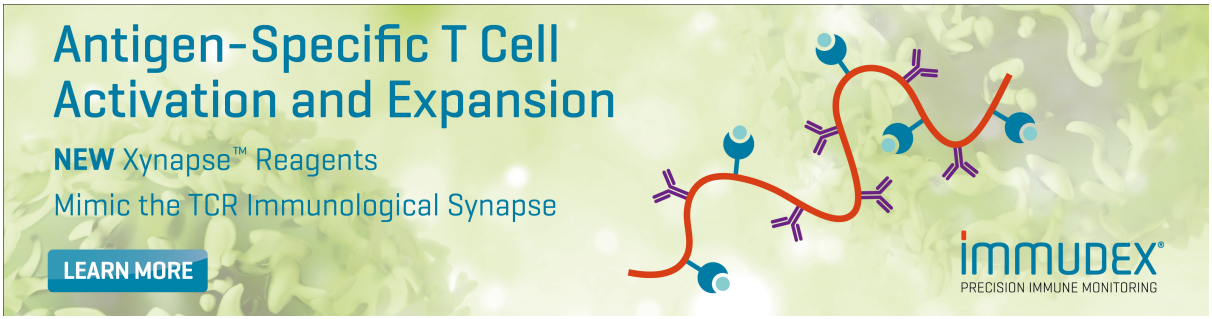

Downloaded from https://academic.oup.com/jimmunol/article/214/10/2585/8240403 by Koc University SK Library (KOC) user on 05 December 2025

The Journal of Immunology, 2025, **214**, 2585–2599
https://doi.org/10.1093/jimmun/vkaf205
Advance access publication August 24, 2025
Research Article

CD20$^+$ natural killer cells are polyfunctional, memory-like cells that are enriched in inflammatory disorders

Özgür Albayrak [1], Ergün Tiryaki [2], Nazan Akkaya [2], Ali Burak Kızılırmak [2], Tansu Doran [2], Gökçe Gökmenoğlu [2], Muhammed Yüksel [1], Bürge Ulukan [2], Mina Üzülmez [3], Işıl Baytekin [3], Önder Kemal Soylu [3], Güneş Esendağlı [4], Ingrid Meinl [5], Mesrure Köseoğlu [3], Burcu Yüksel [3], Suat Erus [6], Çiğdem Arıkan [1,7], Seçil Vural [1,8], Müjdat Zeybel [1,9], Aysun Soysal [3], Edgar Meinl [5,10], and Atay Vural [1,11,*]

[1]Koç University Research Center for Translational Medicine, Koç University, Istanbul, Türkiye
[2]Graduate School of Health Sciences, Koç University, Istanbul, Türkiye
[3]Neurology Department, Bakirkoy Prof. Dr Mazhar Osman Education and Research Hospital for Psychiatric and Neurological Diseases, Istanbul, Türkiye
[4]Department of Basic Oncology, Hacettepe University Cancer Institute, Ankara, Turkiye
[5]Institute of Clinical Neuroimmunology, University Hospital, Ludwig-Maximilians-Universität München, Munich, Germany
[6]Department of Thoracic Surgery, School of Medicine, Koç University, Istanbul, Türkiye
[7]Department of Pediatric Gastroenterology and Organ Transplant, Koç University School of Medicine, Istanbul, Türkiye
[8]Department of Dermatology, Koç University School of Medicine, Istanbul, Türkiye
[9]Department of Gastroenterology and Hepatology, School of Medicine, Koç University, Istanbul, Türkiye
[10]Biomedical Center, Medical Faculty, Ludwig-Maximilians-Universität München, Martinsried, Germany
[11]Department of Neurology, Koç University School of Medicine, Istanbul, Türkiye

*Corresponding author: Department of Neurology, Koç University Research Center for Translational Medicine (KUTTAM), Koç University School of Medicine, Davutpaşa Cad. No: 4, Topkapı/Zeytinburnu, 34010 Istanbul, Turkey. Email: atayvural@ku.edu.tr

Abstract

While CD20 was initially characterized as a B cell–specific marker, its expression on memory T cells has expanded our understanding of this molecule's distribution and function. Here, we identify a previously unrecognized CD20-expressing NK cell population and demonstrate its functional significance. CD56$^+$CD20$^+$ NK cells exhibit hallmarks of cellular activation, including elevated NKp46, CD69, and CD137 expression, enhanced proliferative capacity, and increased production of inflammatory cytokines (IFN-γ, GM-CSF, TNF-α, IL-10). Functional analyses revealed enhanced cytotoxicity against K562 targets, correlating with increased expression of cytolytic mediators including granzymes A, B, and K, perforin, FASL, and TRAIL. Single-cell transcriptional profiling demonstrated that MS4A1-expressing NK cells possess a distinct molecular signature characterized by elevated granzyme K expression and memory-like features. These cells preferentially localize to secondary lymphoid organs and accumulate in inflammatory tissues. Notably, CD56$^+$CD20$^+$ NK cells are enriched in multiple inflammatory conditions, including multiple sclerosis, autoimmune hepatitis, hepatitis B infection, hepatocellular carcinoma, and lung cancer. Treatment with rituximab depletes this population, suggesting potential therapeutic implications. Our findings establish CD20$^+$ NK cells as a functionally distinct lymphocyte subset with enhanced effector capabilities and tissue-homing properties, providing new insights into immune regulation in inflammatory diseases.

Keywords: CD20$^+$ NK cells, cytotoxicity, granzyme K, multiple sclerosis, rituximab

Introduction

CD20 is expressed abundantly on B cells, and depletion of B cells by CD20 monoclonal antibodies has proved to be an effective treatment modality in multiple sclerosis (MS), underscoring their pivotal role in MS pathogenesis.[1] Intriguingly, other B cell–specific treatments like atacicept and belimumab that do not target CD20 have not demonstrated effectiveness in MS, raising the question whether CD20 contributes to MS pathogenesis through mechanisms beyond its presence on B cells.[2]

In addition to B cells, CD20 is expressed at low levels by a fraction of T cells.[3,4] These CD3$^+$CD20$^+$ lymphocytes were shown to have an active phenotype with strong cytokine secretion upon stimulation, are enriched in type 1 cytotoxic CD8$^+$ T cells, and have a predominantly memory T-cell phenotype.[4,5] Moreover, CD20$^+$ T cells are also depleted by CD20 monoclonal antibody therapies, and their depletion was shown to ameliorate experimental autoimmune encephalomyelitis independent of B cells.[6–8] These and other studies demonstrated that CD3$^+$CD20$^+$ cells are clinically relevant in several autoimmune disorders like MS, rheumatoid arthritis, Sjögren syndrome, and psoriasis, and have a role in cancer immunosurveillance.[9,10] It remains, however, unknown whether CD20 expression is restricted solely to cells of the adaptive immune response.

In this study, we report that natural killer (NK) cells also express CD20 on their surface and thus demonstrate that CD20 expression is not limited to adaptive lymphocytes. In addition to having a more active phenotype like CD3$^+$CD20$^+$ cells, CD20$^+$ NK cells exhibit greater degranulation capacity and cytotoxicity against cancer cells. Importantly, CD56$^+$CD20$^+$ cells have a higher proliferative

Received: January 10, 2025. **Accepted:** July 11, 2025
© The Author(s) 2025. Published by Oxford University Press on behalf of The American Association of Immunologists.
This is an Open Access article distributed under the terms of the Creative Commons Attribution-NonCommercial License (https://creativecommons.org/licenses/by-nc/4.0/), which permits non-commercial re-use, distribution, and reproduction in any medium, provided the original work is properly cited. For commercial re-use, please contact reprints@oup.com for reprints and translation rights for reprints. All other permissions can be obtained through our RightsLink service via the Permissions link on the article page on our site—for further information please contact journals.permissions@oup.com.

Downloaded from https://academic.oup.com/jimmunol/article/214/10/2585/8240403 by Koc University SK Library (KOC) user on 05 December 2025

capacity and possess memory-like molecular features. We also show that $CD56^+CD20^+$ cells are enriched in tissues, especially in secondary lymphoid organs. Finally, by examining blood and tissue samples from patients with a wide range of disorders, and publicly available single-cell RNA sequencing (scRNA-seq) datasets, we show that $CD56^+CD20^+$ cells are involved in the pathogenesis of several autoimmune disorders, hepatitis B virus (HBV) infection, and cancer.

Materials and methods

Study population

The neurological cohort of the study was approved by the Koç University Clinical Research Ethics Committee under protocol number 2020.456.IRB1.169. A voluntary informed consent form was signed by all patients and healthy controls. Thirty-one MS, 8 Inflammatory Demyelinating Disorders (IDD), 12 Other Inflammatory Neurological Diseases (OIND), and 15 Non-Inflammatory Neurological Syndromes (NINS) patients and 14 healthy volunteers were included in the study. All patients received their diagnosis from Bakırköy Mazhar Osman Psychiatric Hospital neurology outpatient clinics depending on Expanded Disability Status Scale (EDSS) scores, oligoclonal band electrophoresis results, and functional magnetic resonance imaging scans. Ten milliliters of peripheral blood was drawn into Vacutainer tubes containing K_3EDTA, and cerebrospinal fluid (CSF) was drawn into non-coagulated tubes by lumbar puncture. Samples were transported to Koç University Hospital Research Center for Translational Medicine. Blood and CSF samples of MS and IDD patients were analyzed as the patient population whereas OIND and NINS patients' blood samples were analyzed as disease controls. EDSS scores of MS patients were also collected to be compared with $CD20^+$ NK cell frequencies in both blood and CSF samples.

To determine if $CD56^+CD20^+$ cells are really a subtype of NK cells, we analyzed PBMCs of 12 MS patients before and after 6 months of rituximab treatment. Samples were obtained from the Ludwig Maximillan University (LMU) Institute of Clinical Neuroimmunology and analyzed at the LMU flow cytometry core facility using LSR Fortessa (BD Biosciences, USA).

For the chronic liver disease (CLD) cohort, tissue collection and liver mononuclear cell isolation methods adhered to ethical guidelines. Twenty-seven patients with CLD were enrolled in this study, with approval from the Koç University Ethics Committee under approval numbers 2016.024.IRB2.005 and 2017.139.IRB2.048. Liver specimens were collected from explant livers, and histopathological scoring followed the Ishak pathological staging system. The study population included patients with hepatocellular carcinoma (HCC) alongside viral hepatitis infection, alcohol-related liver disease, or viral hepatitis. Male and female participants with alcohol consumption exceeding 60 g and 40 g per day, respectively, were included in the alcohol-related liver disease cohort. Barcelona clinic liver cancer (BCLC) stage for HCC and FIB-4 scores for all patients with CLD were assessed as part of the analysis.

To assess the presence of CD20-expressing NK cells in autoimmune disorders, 7 pediatric patients with autoimmune hepatitis and 7 age- and sex-matched controls were also included in the study with approval from the Koç University Ethics Committee under approval number 2019.255.IRB2.077. Liver biopsies of healthy controls were also analyzed to determine $CD20^+$ NK cells in liver. Frozen PBMC samples were acquired from the Koç University Hospital Department of Pediatric Hepatology.

Tumor and adjacent healthy tissues from 4 patients with lung cancer at Koç University Hospital were analyzed to observe if $CD20^+$ NK cells were abundant in cancer tissues. For this purpose, tissue samples were homogenized into single-cell suspensions by GentleMACS Octo Dissociator using Human Tumor Dissociation Kit (Miltenyi Biotech, Germany). Patients were enrolled in the study with approval from the Koç University Ethics Committee under approval number 2020.001.IRB2.001.

Apart from the rituximab-treated patient samples, all other samples were analyzed at the Koç University Hospital Research Center for Translational Medicine flow cytometry core facility using Attune NxT Focusing Cytometer (Thermo Scientific, USA). Flow cytometry data were stored as Flow Cytometry Standard files and analyzed by FlowJo version 10.10.0 (BD Biosciences).

PBMC isolation

PBMCs from peripheral blood were isolated using density gradient centrifugation method. Blood samples were diluted 1:1 with staining buffer (PBS containing 1% BSA), carefully layered on equal volume of Lymphoprep d = 1.077 g/mL (Axis-Shield, Norway), and centrifuged at $500 \times g$ for 30 minutes at room temperature (RT) without brake. Buffy coat–containing PBMCs were collected into a sterile 50-mL falcon tube and washed with equal volume of staining buffer at $500 \times g$ for 5 minutes. Supernatant was discarded and, if red blood cells were observed, cell pellet was resuspended with 2 mL of red blood cell lysis buffer (NH_4Cl, Na_2HCO_3, EDTA, pH = 7.3), incubated for 10 minutes at RT, and centrifuged at $500 \times g$ for 5 minutes. After centrifugation, cell pellet was resuspended with 1 mL of staining buffer and counted on Sysmex XE-2100 Automated Cell Counter (Roche, Germany). 1×10^7 cells was cryopreserved in liquid nitrogen whereas 6×10^6 cells was used in immunophenotyping experiments.

Liver mononuclear cell isolation

Mononuclear cells from explanted livers were isolated using a nonenzymatic method paired with Ficoll gradient separation. The liver tissue was finely minced into smaller fragments. Serum-free RPMI 1640 medium was added to a stomacher bag containing the minced tissue, which was then incubated in a Stomacher machine (Seward Laboratory Systems, United Kingdom) to facilitate cell release. After incubation, the cell mixture was extracted from the Stomacher bag and filtered through a 125-μm nylon mesh. The filtrate was subjected to washing steps, and the resulting pellet was resuspended in 1× DPBS (Thermo Scientific). The cell suspension was gently layered over Lymphoprep (density: 1.077 g/mL, Axis-Shield) to create a distinct separation layer followed by centrifugation. An additional washing step was performed to remove residual Lymphoprep. Finally, the pellet was resuspended in a freezing medium of 90% FBS and 10% DMSO for cryopreservation.

Preparation of CSF samples

CSF samples were centrifuged at $400 \times g$ for 15 minutes at 4 °C. After centrifugation, CSF fluids were put into −80 °C

Downloaded from https://academic.oup.com/jimmunol/article/214/10/2585/8240403 by Koc University SK Library (KOC) user on 05 December 2025

for further use and pellets were used to determine $CD20^+$ NK cells.

Culturing of K562 cells

K562 human myeloid leukemia cell line (ATCC, CCL-243) was cultured in DMEM containing 10% FBS and 1% penicillin-streptomycin (Gibco) at 37 °C in a 5% CO_2 incubator for 3 days. Cells were harvested upon reaching ~85% confluence and 5×10^6 cells was used for downstream applications while remaining cells were cryopreserved in liquid nitrogen for further use.

Immunophenotyping of $CD56^+CD20^+$ NK cells

Presence of $CD56^+CD20^+$ cells were determined by flow cytometric immunophenotyping. PBMC, CSF, and homogenized tissue samples were placed into 3 tubes. Cells in the first tube were used as unstained negative control. The second tube was stained with anti-human CD3, CD56, CD14, CD19, and Zombie NIR Fixable Viability Dye (FVD), and the third tube was stained with the full antibody panel. Table S17 shows the brands, clones, and conjugated fluorochromes of antibodies used in the experiment. Samples were incubated with antibodies for 20 minutes in the dark and washed with 2 mL of staining buffer at $500 \times g$ for 5 minutes. Supernatant was discarded and cells were resuspended with 1 mL of staining buffer and analyzed under Attune NxT Focusing Cytometer (Thermo Scientific). 1×10^6 cells for PBMCs and all of the cells in CSF were analyzed within the Lymphocyte gate in FSC × SSC plot. FlowJo version 10.10.0 software (BD Biosciences) was used to analyze the results.

Functional analysis of $CD56^+CD20^+$ cells

Ten cryopreserved PBMCs were thawed in a 37 °C water bath, taken into complete medium (RPMI 1640 + 10% FBS + 1% penicillin-streptomycin, Gibco), and rested overnight at 37 °C in a 5% CO_2 incubator. $CD56^+$ NK cells were isolated from PBMCs by using MojoSort Human $CD56^+$ NK Isolation Kit (BioLegend) according to the manufacturer's instructions. Isolated $CD56^+$ cells were seeded into 96-well round-bottom plates at a density of 1×10^5 cells/100 µL and stimulated with Cell Activation Cocktail (PMA/ionomycin without Brefeldin A, BioLegend), IL-2 (10 ng/mL) and IL-15 (10 ng/mL) (BioLegend), and 1×10^5 K562 cells/100 µL with IL-2/IL-15 for 1 hour at 37 °C in a 5% CO_2 incubator, respectively. After 1 hour, Brefeldin A (BioLegend) was added into the wells and an additional stimulation was carried out for 5 hours. Two sets of antibody panels were used to determine the functions of $CD20^+$ NK cells (Table S18). Results were analyzed by FlowJo version 10.10.0 software (BD Biosciences).

K562 killing assay

First, 1×10^4 $CD20^+$ and $CD20^-$ NK cells from PBMCs of healthy controls was sorted with FACS Aria III Cell Sorter (BD Biosciences) and cell purity and viability were then determined. The experiment was continued if <95% purity and viability were achieved. K562 cells were labeled with CFSE (BioLegend) according to the manufacturer's instructions. Sorted NK cells and labeled K562 cells were co-cultured in a 96-well round-bottom plate at a 2.5:1 E:T ratio in complete RPMI medium for 6 hours at 37 °C in a 5% CO_2 incubator with the presence of recombinant human IL-2 (10 ng/mL) and IL-15 (10 ng/mL) (BioLegend). After incubation, samples were centrifuged once at $500 \times g$ for 5 minutes. Supernatants were collected and later used for multiplex cytokine analysis. Cells were stained with Annexin V PE Apoptosis Detection Kit with 7-AAD (BioLegend) according to the manufacturer's instructions.

CFSE-stained K562 cells were gated, and apoptosis was determined by measuring only Annexin V for early apoptosis, Annexin V^+7AAD^+ for late apoptosis, and $7AAD^+$ for nonapoptotic cell death. Materials used in the study are given in Table S19. Results were analyzed by FlowJo version 10.10.0 software (BD Biosciences).

Measurement of inflammatory molecules secreted by NK cells

Supernatants collected during the K562 killing assay were used to determine the concentration of TNF-α, IFN-γ, granzyme A (GrA), granzyme B (GrB), perforin, granulysin, sFas, and sFasL molecules secreted from $CD20^+$ and $CD20^-$ NK cells by using the 13plex LegendPlex Human CD8/NK Kit (BioLegend) according to the manufacturer's instructions. In brief, standards and samples were combined with APC-conjugated premixed beads coated with capture antibodies in a 96-well round-bottom plate and incubated at RT for 2 hours. After incubation, plate was centrifuged with wash buffer and beads were resuspended with detection antibodies for 1 hour. Streptavidin-PE was added onto the wells and plate was incubated for another 30 minutes. Finally, plate was centrifuged and resuspended with 200 µL wash buffer. Resuspended beads were transferred into 12 × 75-mm 5 mL tubes and an additional 300 µL of wash buffer was added. Cytokine standards and samples were run under Attune NxT Acoustic Cytometer (Thermo Fisher). Beads were gated with FSC vs SSC plot whereas APC vs PE plot was used to classify beads and record mean fluorescence intensity (MFI) values for each cytokine. Collected data were analyzed with LegendPlex Analysis software version 8.0 (BioLegend).

NK cell proliferation assay

PBMCs from 8 healthy control subjects were included in the NK proliferation studies. 1×10^7 PBMCs were stained with CFSE Cell Division Tracker Kit according to the manufacturer's instructions. After staining, 1×10^6 cells were seeded into 96-well U-bottom plates as day 2, day 4, and day 7 with unstimulated and stimulated wells. Then, 10 ng/mL IL-2 and 10 ng/mL IL-15 (BioLegend) were added to stimulated wells and plates were placed in a 5% CO_2 incubator at 37 °C. Samples were stained after the second, fourth, and seventh days with Zombie NIR FVD, mouse anti-human CD20 PE (clone 2H7), CD19 APC (clone HIB19), CD56 PE-Cy5 (clone MEM-188), CD3 APC-Cy7 (clone SK7), and CD14 APC-Cy7 (clone HCD14).

In another set of proliferation assays, PBMCs from 8 healthy subjects were first stained with CFSE Cell Division Tracker Kit and further stained with Zombie NIR FVD, mouse anti-human CD20 PE (clone 2H7), CD19 APC-Cy7 (clone HIB19), CD56 APC (clone HCD56), CD3 APC-Cy7 (clone SK7), and CD14 APC-Cy7 (clone HCD14). $CD20^+$ and $CD20^-$ NK cells were sorted with a Cytoflex SRT cell sorter (Beckman-Coulter) in purity setting with 100 µm nozzle and a speed of 1,500 events/second. Sorting purity was determined by flow cytometry and >95% pure samples were included in the study. $CD20^+$ and $CD20^-$ NK cells were seeded into 96-well U-bottom plates at day 2, day 4, and day

Downloaded from https://academic.oup.com/jimmunol/article/214/10/2585/8240403 by Koc University SK Library (KOC) user on 05 December 2025

7. Next, 10 ng/mL IL-2 and 10 ng/mL IL-15 (BioLegend) were added to stimulated wells and plates were placed in a 5% CO_2 incubator at 37 °C. Samples were restained after the second, fourth, and seventh days with the same aforementioned FVDs and antibodies, acquired with Cytoflex SRT (Beckman-Coulter), and proliferation modeling analyses were done by FlowJo version 10.10.0 software (BD Biosciences). All antibodies, FVDs, and CFSE Cell Division Tracker Kit were purchased from BioLegend.

scRNA-seq data analysis

All datasets were analyzed using the Scanpy pipeline.

Twin MS dataset

The study by Ingelfinger et al contains peripheral blood samples from twins concordant with MS.[11] The study is composed of 2 sorting schema, $CD3^+CD4^+$ Th cells, and $CD3^-CD11c^+$ myeloid cells. The same quality control filters with the original article were applied. Scrublet is used for doublet detection.[23] The dataset is normalized to 10,000 and then $\log(x+1)$ transformation is applied. Principal component analysis (PCA) has been computed after dataset is scaled to zero mean and unit variance using Scanpy's PCA function with arpack solver. Batch correction is performed with the Harmony algorithm on the principal components and the subsequent neighborhood graph is computed on the first 50 Harmony-corrected principal components.[24] Clustering is performed with Leiden algorithm by setting the resolution to 0.3 to catch main NK subtypes.[25]

COVID-19 dataset

The dataset of the COMBAT consortium was downloaded as the processed AnnData object from Zenodo.[12] NK cells were selected based on the original report's annotations. Then differential gene expression (DGE) analysis was conducted using Wilcoxon rank-sum statistics with Benjamini–Hochberg correction. Calculations were carried with "sc.tl.rank_genes_groups" function of Scanpy. Since these data were created with the Cellular Indexing of Transcriptomes and Epitopes by Sequencing (CITE-seq) protocol, both antibody-derived tags (ADTs) and RNA were available. DGD analysis was conducted for both RNA and ADT assays. CD20 expression of cells was determined using RNA assay and the cells were compared using this annotation for the ADT assay, as well. The differential expression analysis of both RNA and ADT assays was calculated using Wilcoxon rank-sum test.

Melanoma dataset

The raw count matrix of the data by de Andrade et al was accessed from Gene Expression Omnibus with the accession number GSE139249.[14] During the preprocessing of the dataset, cells were removed if containing <200 genes and genes were removed if expressed as <3 cells. Doublets were identified and removed using Scrublet.[23] Data were normalized to 1,000 and $\log(x+1)$ transformed. PCA was calculated on the data layer that was scaled to zero mean and unit variance. Batches were integrated using the Harmony algorithm. The neighborhood graph was computed by Scanpy using the default uniform manifold approximation and projection (UMAP) kernel on Harmony-corrected principal component space. Contaminating cells were removed in initial clustering through both manual inspection of clusters and automated cell type prediction using CellTypist's "Immune_High_All.pkl" model.[15] Additionally, the majority voting classifier was enabled to increase classification accuracy.

Cross-tissue immune cell dataset

Data by Domínguez Conde et al were downloaded from the tissue Immune Cell Atlas website.[15] Preprocessed AnnData object was used for the downstream tasks. Since the additional training data for CellTypist were curated from the literature and the count matrix was not available, we took another approach to remove B cells that may potentially contaminate NK cells. Gene set score was calculated using a set of B-cell markers using the "sc.tl.score_genes" function. The cutoff was set to zero and all cells with a B-cell gene signature were removed. After that, $CD20^+$ vs $CD20^-$ NK cells were compared using "sc.tl.rank_genes_groups" function as a validation. No B-cell genes were upregulated among the $CD20^+$ NK cell population.

WGCNA analysis

Weighted gene coexpression analysis (WGCNA) analysis was conducted on highly variable genes detected by Scanpy's "highly_variable_genes" function. A signed hybrid network was conducted using the pyWGCNA package.[26] Modules were visualized with igraph network analysis software.[27]

Gene set enrichment analysis

Gene set enrichment analysis (GSEA) with hypergeometric enrichment test was performed with EnrichR using upregulated genes from differential gene expression analysis.[28] "BioCarta_2016," "GO_Biological_Processes_2023," and "GO_Cellular_Components_2023" libraries were used for testing. Plots are generated using Seaborn and Matplotlib.

Statistical analysis

$CD56^+CD20^+$ cell population percentages were compared between the healthy control (HC), MS, IDD, OIND, and NINS groups; functional, K562 cytotoxicity, and cytotoxic molecule analysis between $CD56^+CD20^+$ and $CD56^+CD20^-$ cells, as well as autoimmune hepatitis PBMCs, Bone Marrow, tumor, and healthy tissue immunophenotyping analysis, were done by Mann–Whitney *U* rank-sum test. Comparison of proliferative capacities between sorted $CD56^+CD20^+$ and $CD56^+CD20^-$ cells was done using repeated-measures one-way ANOVA with Bonferroni correction. Analysis in blood and CSF was done by Spearman correlation. GraphPad version 10.4.2 was used as statistical analysis software.

Results

CD20 expression on NK cells

In a cohort of HCs (mean age, 30.3 ± 1.3 years; 9 female and 5 male), we observed that 1% to 4.5% of peripheral blood NK cells express CD20 at a frequency similar to that of $CD3^+CD20^+$ T cells (median [interquartile range {IQR}], 3.3 [2.4–3.9] vs 4.4 [3.7–5], respectively) (Fig. 1A, B). CD20 was present on both $CD56^{bright}$ and $CD56^{dim}$ cells, the ratio being higher in the former (median [IQR], 4.2 [3.5–5.1] vs 2.9 [1.9–3.5], respectively) (Fig. 1B).

Downloaded from https://academic.oup.com/jimmunol/article/214/10/2585/8240403 by Koc University SK Library (KOC) user on 05 December 2025

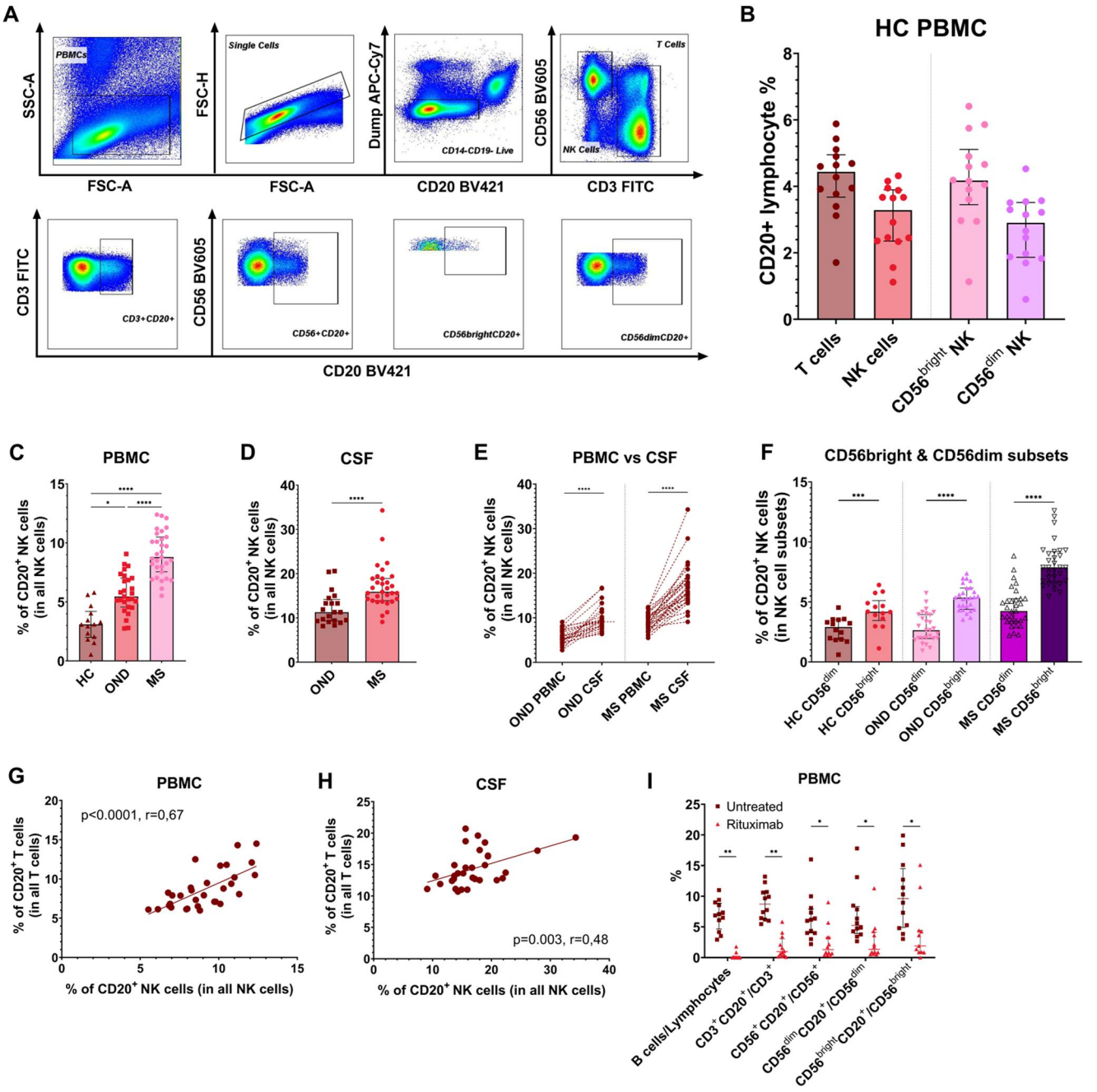

Figure 1. (A) Gating strategy of live $CD3^-CD14^-CD19^-CD56^+CD20^+$ cells. (B) The frequency distribution of $CD20^+$ NK cells and T cells in the blood of healthy volunteers. (C) The ratio of $CD20^+$ NK cells to all NK cells ($CD56^+CD20^+$ %) is greater in the blood of people with newly diagnosed multiple sclerosis (pwMS, n = 31) compared to the patients with other neurological disorders (OND, n = 27) and healthy controls (HCs, n = 14). *P* values were calculated using Kruskal–Wallis test with Dunn multiple comparisons post hoc correction. (D) The ratio of $CD56^+CD20^+$ cells is higher in the CSF of pwMS compared to patients with OND. *P* value was calculated using 2-tailed Mann–Whitney test. (E) CSF is enriched for $CD56^+CD20^+$ cells compared to the blood in both patient groups. (F) $CD56^{bright}$ NK cells are enriched for $CD20^+$ cells in both HCs and neurological patients. *P* values were calculated using 2-tailed Wilcoxon matched-pairs signed rank test. (G and H) Frequency of $CD56^+CD20^+$ cells in the peripheral blood (G) and CSF (H) of pwMS is correlated with that of $CD3^+CD20^+$ cells in both tissues. *P* and *r* values were calculated by Pearson correlation test. (I) $CD56^+CD20^+$ cells are depleted alongside with B cells and $CD3^+CD20^+$ cells after rituximab treatment compared to untreated pwMS. $^*P < 0.05$, $^{**}P < 0.01$, $^{***}P < 0.001$, $^{****}P < 0.0001$.

The percentage of $CD20^+$ NK cells is higher in the blood and CSF of people with MS compared to controls

In a previous study, the percentage of $CD20^+$ T cells was reported to be increased in the peripheral blood and CSF of people with MS (pwMS), and this increase was found to be related to disease severity.[5] We asked whether the frequency of $CD56^+CD20^+$ cells is also increased in pwMS and answered this question by analyzing the paired peripheral blood and CSF of a cohort of patients with new onset of neurological symptoms, including a demyelinating attack (Table S1).

We found that the ratio of $CD20^+$ NK cells to all NK cells is significantly higher in pwMS (mean ± SD, 9 ± 1.9) compared to people with other neurological disorders (ONDs) (5.7 ± 1.6,

Downloaded from https://academic.oup.com/jimmunol/article/214/10/2585/8240403 by Koc University SK Library (KOC) user on 05 December 2025

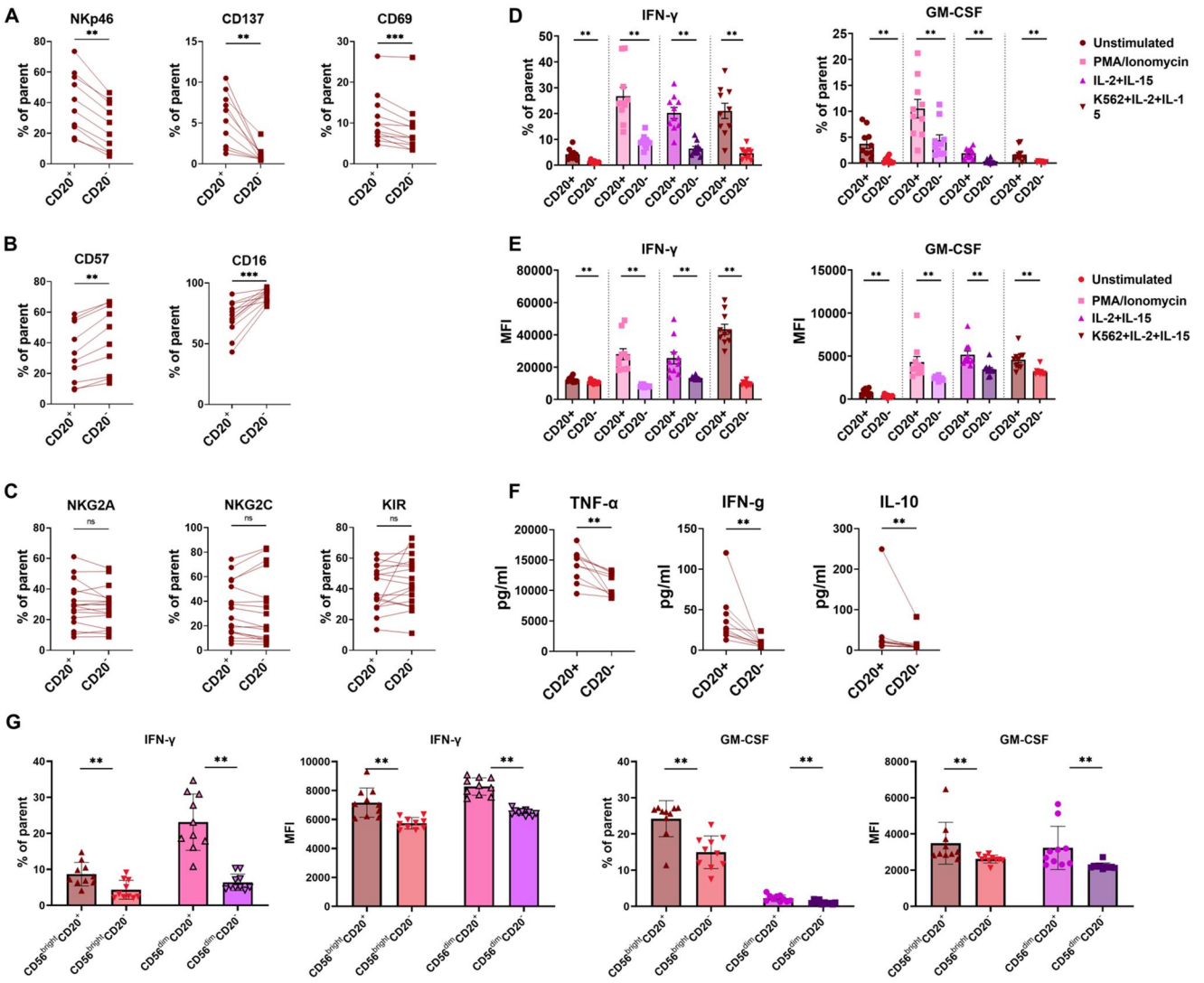

Figure 2. CD20$^+$ NK cells have a more active phenotype and secrete more cytokines. (A and B) The ratio of NKp46-, CD69-, and CD137-expressing cells are higher among CD20$^+$ NK cells (A), whereas the ratio of CD57$^+$ and CD16$^+$ cells is higher among CD20$^-$ NK cells (B). (C) The percentage of NKG2A-, NKG2C- and KIR-expressing cells are similar in both groups. (D and E) Intracellular staining and flow cytometry analysis of sorted NK cells from healthy donors revealed that the percentage of cells producing IFN-γ and GM-CSF (D) and the amount produced, as shown by MFI measurements (E), are higher in CD56$^+$CD20$^+$ cells after stimulation with PMA/ionomycin, IL-2 plus IL-15, and K562 cells plus IL-2 plus IL-15. (F) Concentrations (pg/mL) of TNF-α, IFN-γ, and IL-10 were measured in supernatants collected after a 6-hour co-culture of sorted CD20$^+$ or CD20$^-$ NK cells with K562 target cells (2.5:1 E:T ratio) in the presence of IL-2 and IL-15. Measurements were performed using a multiplex bead array (see details in the Materials and methods). Results show significantly higher secretion of TNF-α, IFN-γ, and IL-10 by CD20$^+$ NK cells compared to CD20$^-$ NK cells under these stimulation conditions. (G) Subgroup analysis of cells stimulated with IL-2 plus IL-15 showed that the ratio and MFI of IFN-γ and GM-CSF expression are higher in both CD56^{bright}CD20$^+$ and CD56^{dim}CD20$^+$ cells, compared to their CD20$^-$ counterparts. *P* values were calculated using 2-tailed Wilcoxon matched-pairs signed-rank test. $^{**}P < 0.01$, $^{***}P < 0.001$; ns, not significant.

$P < 0.0001$) and HCs (3.2 ± 1.5, $P < 0.0001$) in the peripheral blood. Similarly, the percentage of CD20$^+$ NK cells was higher in the CSF of pwMS (17 ± 4.9) compared to people with OND (12.2 ± 3.7, $P < 0.0001$) (Fig. 1C, D). Clinical features of the study participants are shown in Table S1. CD20$^+$ NK cells were enriched in CSF compared to peripheral blood in all patients (Fig. 1E). CD56$^+$CD20$^+$ cells were more frequent in the CD56^{bright} population compared to CD56^{dim} (Fig. 1F). In addition, the frequency of CD56$^+$CD20$^+$ cells was significantly correlated with that of CD3$^+$CD20$^+$ cells and B cells in pwMS in both the peripheral blood ($P < 0.0001$ and $P < 0.05$, respectively) and CSF ($P < 0.01$ and $P < 0.01$, respectively) (Fig. 1G, H; Fig. S1A, B).

CD20$^+$ NK cells in blood are depleted after rituximab therapy

Both B cells and CD20$^+$ T cells are known to be depleted after rituximab infusion and CD3$^+$CD20$^+$ cells were shown to replenish before B cells.[4] We compared the ratio of CD56$^+$CD20$^+$ cells obtained from 12 rituximab-treated (median, 1.3 [IQR, 0.5–3.3]) and 12 untreated (median, 6 [IQR, 4–7.9]) pwMS and found significantly lower CD56$^+$CD20$^+$ cell frequency in the rituximab group ($P < 0.05$). Moreover, the CD56$^+$CD20$^+$ cell ratio was higher compared to B cells in treated patients, indicating that CD20$^+$ NK cells may also repopulate faster than B cells (Fig. 1I).

Downloaded from https://academic.oup.com/jimmunol/article/214/10/2585/8240403 by Koc University SK Library (KOC) user on 05 December 2025

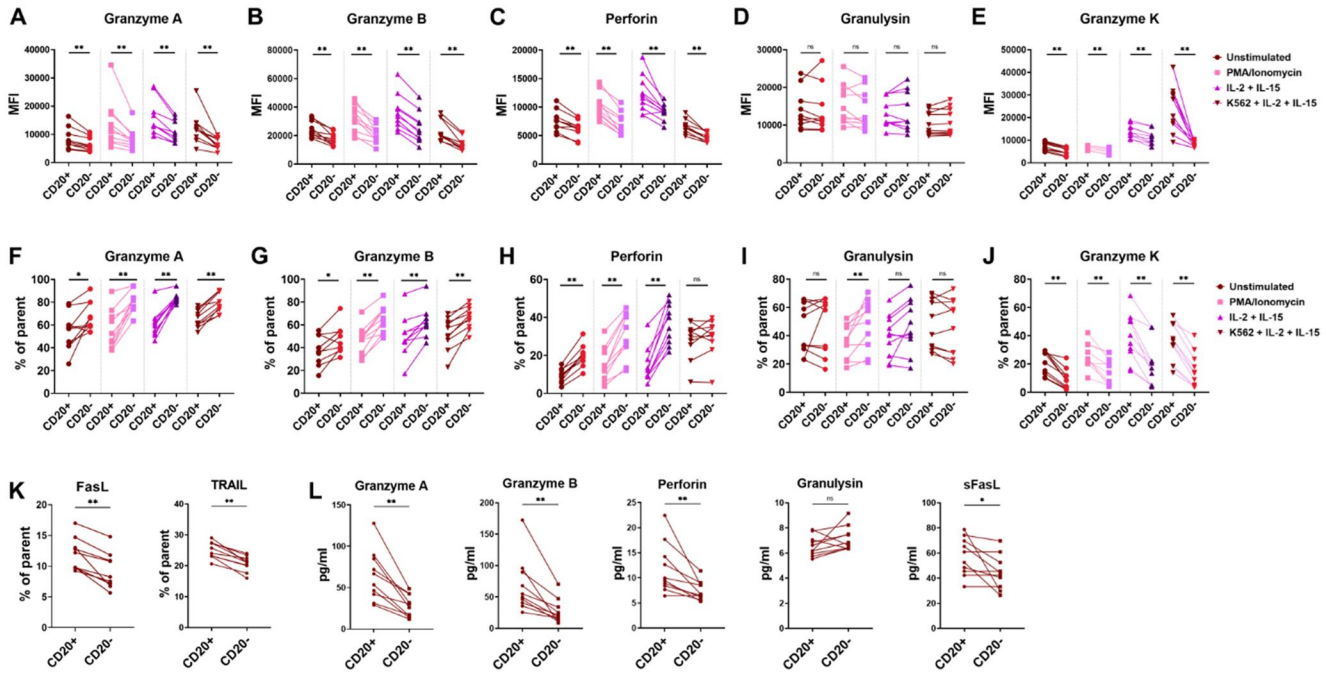

Figure 3. CD20$^+$ NK cells produce and secrete cytotoxic molecules more abundantly. (A–E) The amount of GrA, GrB, perforin, and GrK but not granulysin produced by CD20$^+$ NK cells is higher compared to CD20$^-$ NK cells, especially after stimulation. (F–J) However, only the percentage of GrK expression is higher among CD20$^+$ NK cells, whereas the ratios of GrA-, GrB-, and perforin-expressing cells are higher among CD20$^-$ NK cells. (K) A greater proportion of the CD56$^+$CD20$^+$ cells express FasL and TRAIL on the cell surface. (L) Concentrations (pg/mL) of GrA, GrB, perforin, granulysin, soluble FasL (sFasL), and soluble Fas (sFas) were measured in supernatants collected after a 6-hour co-culture of sorted CD20$^+$ or CD20$^-$ NK cells with K562 target cells in the presence of IL-2 and IL-15, using a multiplex bead array. Results show significantly higher secretion of these mediators by CD20$^+$ NK cells compared to CD20$^-$ NK cells under these conditions. *P* values were calculated using 2-tailed Wilcoxon matched-pairs signed-rank test. *$P < 0.05$, **$P < 0.01$; ns, not significant.

CD20$^+$ NK cells have a more active phenotype and secrete more cytokines

After recognizing the significance of CD20$^+$ NK cells in MS, we aimed to elucidate the phenotype and functional characteristics of these cells in both resting conditions and after stimulation.

We found that a higher percentage of CD20$^+$ NK cells express the activating receptor NKp46 ($P < 0.01$) and activation markers CD137 ($P < 0.01$) and CD69 ($P < 0.001$) compared to CD56$^+$CD20$^-$ cells, whereas the ratio of CD57$^+$ ($P < 0.01$) and CD16$^+$ ($P < 0.001$) cells was higher among CD20$^-$ NK cells (Fig. 2A, B). The percentage of NKG2A-, NKG2C-, and KIR-expressing cells was similar in both groups (Fig. 2C).

Next, we assessed sorted NK cells from healthy donors by intracellular staining for their cytokine production capacity under 3 different stimulation conditions: PMA/ionomycin, IL-2 plus IL-15, and K562 cells plus IL-2 plus IL-15. The percentage of cells producing IFN-γ and GM-CSF was higher in CD56$^+$CD20$^+$ cells under all conditions ($P < 0.01$ for all conditions tested for both cytokines) (Fig. 2D). The MFI of these cytokines was also higher in CD56$^+$CD20$^+$ cells ($P < 0.01$ for all conditions tested for both cytokines) (Fig. 2E). Moreover, CD56$^+$CD20$^+$ cells stimulated with K562 cells plus IL-2 and IL-15 secreted more TNF-α ($P < 0.01$), IFN-γ ($P < 0.01$), and IL-10 ($P < 0.01$) into the cell culture medium compared to the CD20$^-$ NK cells (Fig. 2F).

Subgroup analysis of the CD56^{bright} and CD56^{dim} populations revealed that both the percentage of NK cells expressing IFN-γ and GM-CSF as well as their MFI levels are higher in CD56^{bright}CD20$^+$ and CD56^{dim}CD20$^+$ cells compared to their CD20$^-$ counterparts (Fig. 2G).

The percentage of CD56$^+$CD20$^+$ cells among CD56$^+$ NK cells and the MFI of CD20 were not changed after 6 hours under either of the stimulation conditions (Fig. S2A, B).

CD20$^+$ NK cells produce and secrete greater quantities of cytotoxic molecules

NK cells are critical for the elimination of virally infected and cancerous cells. Therefore, we next investigated the production of cytotoxic molecules by CD56$^+$CD20$^+$ cells during incubation with K562 cancer cells under IL-2 plus IL-15 stimulation. We found that the MFIs of GrA, GrB, perforin, and granzyme K (GrK), but not granulysin, were higher in CD20$^+$ NK cells compared to CD20$^-$ NK cells in the resting condition and after stimulation (Fig. 3A–E).

Conversely, the percentage of cells expressing GrA, GrB, and perforin was lower in CD56$^+$CD20$^+$ cells compared to CD20$^-$ NK cells (Fig. 3F–H). There was no significant difference in the ratio of granulysin-expressing cells between the 2 groups (Fig. 3I). For GrK, the ratio was higher among CD56$^+$CD20$^+$ cells (Fig. 3J). These results are in line with our data showing that CD20$^+$ NK cells are relatively more common among CD56^{bright} NK cells. Of note, further analysis revealed that the GrK$^+$ cell ratio was similar and close to 100% in both CD56^{bright}CD20$^+$ and CD56^{bright}CD20$^-$ cells (Fig. S3A, C), whereas a higher ratio of CD56^{dim}CD20$^+$ cells expressed GrK compared to CD56^{dim}CD20$^-$ cells (Fig. S3B, D).

Downloaded from https://academic.oup.com/jimmunol/article/214/10/2585/8240403 by Koc University SK Library (KOC) user on 05 December 2025

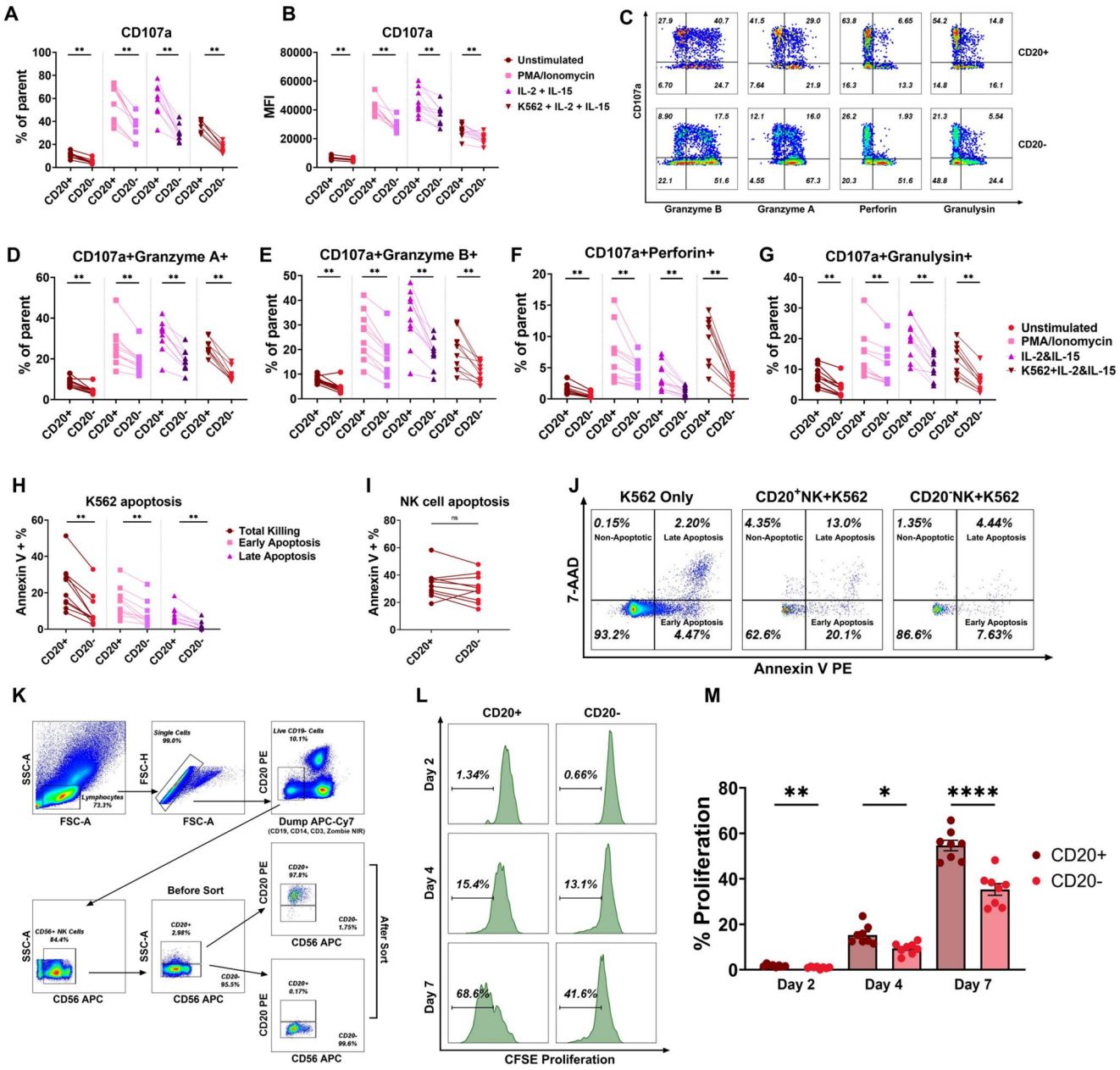

Figure 4. CD20$^+$ NK cells are more efficient killers and have a higher capacity for proliferation after stimulation. (A) A higher percentage of CD20$^+$ NK cells degranulate (CD107a$^+$) after stimulation, and (B) the degranulation capacity (CD107a MFI) of individual CD20$^+$ NK cells is higher. (C) Representative intracellular staining of cytotoxic granule content in degranulating (CD107a$^+$) CD20$^+$ vs CD20$^-$ NK cells. (D–G) Degranulating CD20$^+$ NK cells have a higher content (% positive) of GrA (D), GrB (E), perforin (F), and granulysin (G) compared to CD20$^-$ NK cells. (H) CD20$^+$ NK cells are more efficient killers compared to CD20$^-$ NK cells. Sorted CD20$^+$ or CD20$^-$ NK cells were co-cultured with CFSE-labeled K562 target cells (2.5:1 E:T ratio) for 6 hours in the presence of IL-2 and IL-15 (10 ng/mL each). Apoptosis of K562 cells was measured by Annexin V/7-AAD staining, showing percentages of early apoptotic (Annexin V$^+$/7-AAD$^-$), late apoptotic (Annexin V$^+$/7-AAD$^+$), and total apoptotic (Annexin V$^+$) cells. (I) The rate of apoptosis (% Annexin V$^+$) is similar between sorted CD20$^+$ and CD20$^-$ NK cells following the 6-hour co-culture described in (H). (J) Apoptosis of K562 cells was measured by Annexin V/7-AAD staining, showing percentages of early apoptotic (Annexin V$^+$/7-AAD$^-$), late apoptotic (Annexin V$^+$/7-AAD$^+$), and total apoptotic (Annexin V$^+$) cells. (K) Representative flow cytometry gating strategy of CD20$^+$ and CD20$^-$ NK cell sorting. Total PBMCs from 8 healthy subjects were labeled with CFSE prior to sorting and stimulation with IL-2 and IL-15 (10 ng/mL each). CFSE dilution was assessed at days 2, 4, and 7 within the indicated live NK cell subgroups (CD20$^+$, CD20$^-$), gated at the time of harvest. (L) Representative results for the NK cell proliferation assay. (M) Sorted CD20$^+$ NK cells show a higher percentage of proliferating cells compared to sorted CD20$^-$ NK cells following IL-2 and IL-15 stimulation. *P* values were calculated using repeated-measures one-way ANOVA with Bonferroni correction (L). $^*P < 0.05$, $^{**}P < 0.01$, $^{***}P < 0.001$, $^{****}P < 0.0001$; ns, not significant.

We also found that a greater proportion of the CD56$^+$CD20$^+$ cells express the death-inducing ligands FasL and TRAIL on the cell surface (Fig. 3K).

In line with the above findings, CD56$^+$CD20$^+$ cells secreted higher amounts of GrA, GrB, perforin, soluble FasL, and soluble Fas into the cell culture medium after cytokine stimulation (Fig. 3L).

CD20$^+$ NK cells have a higher capacity of degranulation and are more effective at killing K562 leukemia cells

To investigate the functional consequences of these findings, we first performed a CD107a degranulation assay. We discovered that the percentage of degranulating cells was 2 times higher

Downloaded from https://academic.oup.com/jimmunol/article/214/10/2585/8240403 by Koc University SK Library (KOC) user on 05 December 2025

among $CD20^+$ NK cells compared to $CD20^-$ NK cells after incubation with K562 cells (median [IQR], 37.1 [30.1–41.2] vs 16.6 [13–19]) (Fig. 4A). Furthermore, the degranulation capacity of individual $CD20^+$ NK cells was found to be significantly higher as revealed by MFI of the cell surface CD107a molecules measured after stimulation (median [IQR], 25,636 [23,568–29,864] vs 19,655 [17,674–21,876]) (Fig. 4B).

We also analyzed the frequency of GrA-, GrB-, perforin-, and granulysin-expressing cells among degranulated cells. We found that degranulating $CD20^+$ NK cells contain a higher ratio of all 4 cytotoxic molecules compared to $CD20^-$ NK cells (Fig. 4C–G). These findings show that CD20 expression is associated with superior degranulation capacity for cytotoxic molecules in NK cells.

Next, we performed a killing assay with K562 cells cocultured with either sorted $CD20^+$ or $CD20^-$ NK cells to directly compare their cytotoxic efficacy. Indeed, $CD20^+$ NK cells were found to be more efficient killers compared to $CD20^-$ NK cells ($P < 0.01$) (Fig. 4H). We also measured the ratio of NK cells that undergo apoptosis to see if $CD20^+$ NK cells are more prone to cell death after activation. We did not detect any difference between $CD20^+$ and $CD20^-$ NK cells (Fig. 4I).

$CD20^+$ NK cells have a higher proliferative capacity under IL-2 and IL-15 stimulation

Finally, we sorted $CD20^+$ and $CD20^-$ NK cells from CFSE-labeled HC PBMCs (Fig. 4K) and stimulated them with IL-2 and IL-15 to assess the proliferation capacity of given NK cell subtypes at days 2, 4, and 7. We found that $CD20^+$ NK cells exhibited a higher proliferation capacity at all time points measured ($P < 0.01$ at day 2, $P < 0.05$ at day 4, and $P < 0.0001$ at day 7) compared to their $CD20^-$ counterparts (Fig. 4L, M).

In a separate set of experiments, we replicated the NK cell proliferation assay with PBMCs from HCs with IL-2 and IL-15 for 7 days. We found that $CD20^+$ NK cells have a higher proliferative capacity in response to cytokine stimulation ($P < 0.05$ at days 2, 4, and 7) (Fig. S4A, B). Moreover, the $CD20^+$ NK cell ratio increased gradually ($P < 0.001$, Fig. S4C). As expected, $CD56^{bright}$ cells proliferated more in both $CD20^+$ and $CD20^-$ cell groups (Fig. S4D).

Molecular features of $CD56^+CD20^+$ cells

So far, we have identified that $CD56^+CD20^+$ cells are highly functional cells with increased proliferative capacity and are expanded in neurological disorders, especially MS. Increased functionality and proliferative capacity are characteristic features of memory-like NK cells. To gain more insight into the molecular underpinnings of these characteristics, we analyzed selected publicly available scRNA-seq datasets generated from patients with inflammatory conditions.

First, we analyzed data from the Twin-MS study, in which frozen PBMCs obtained from 8 MS and non-MS monozygotic twin pairs and 2 healthy samples were used.[11] This dataset was created by scRNA-seq of sorted $CD3^+CD4^+$ and $CD3^-CD11c^+$ cells. The dataset contains 56,801 NK cells, and 1,614 (2.84%) of these cells had *MS4A1* expression, the gene coding for CD20. The percentage of *MS4A1*-expressing NK cells was 3.2% in twins with MS and 2.6% in twins without MS. The percentage of *MS4A1*-expressing cells was highest in the $CD56^{bright}$-like cluster that is characterized by high *GZMK* expression (7.44%), followed by proliferating NK cell (2.96%) and $CD56^{dim}$-like (1.39%) clusters (Fig. 5A–E). The analysis of differentially expressed genes between NK cell subclusters verified the presence of *MS4A1* among the top upregulated genes in the $CD56^{bright}$-like cluster (Table S2).

Next, we performed DGE analysis of *MS4A1* expressing NK cells compared to other NK cells. We found that expression of *GZMK*, in addition to the genes encoding for cytokine receptors (*IL7R*, *IL18R1*, *IL18RAP*, *IL4R*, *IL10R*, *IL12RB2*, *IL2RB*, *IL2RG*), NK cell receptors (*KLRC1*, *KLRC2*, *KLRC3*, *KLRC4*, *KLRD1*, *KLRK1*, *KIR2DL4*), TNF receptors (*CD27*, *TNFRSF11A*, *TNFRSF18*), and NK cell memory–related surface markers (*SELL*, *CD44*, *CD2*, *CD52*, *CD3E*, *HLA-DR*) are increased in *MS4A1*-expressing NK cells (Fig. 5F, Table S3). On the other hand, the genes belonging to mature NK cells such as *TBX21*, *PRDM1*, *GZMA*, *GZMB*, *PRF1*, *FCGR3A*, *NKG7*, *KLRG1*, *CX3CR1*, *S1PR5*, *CCL3*, *CCL4*, *CCL5*, and the genes coding for inhibitory receptors such as *TIGIT*, *HAVCR3*, *CD160*, and inhibitory KIR receptors were downregulated (Fig. 5F, Table S3). An analysis of gene ontology for the upregulated genes in MS4A1-expressing NK cells unveiled several significant biological pathways. These pathways encompassed cytoplasmic translation machinery, leukocyte cytotoxicity, assembly of MHC class II protein complexes, cell adhesion, and intracellular signal transduction molecules (Table S4). GSEA of the upregulated genes in MS4A1-expressing NK cells indicated the activation of pathways associated with RAS-independent NK cell–mediated cytotoxicity and signaling induced by bioactive peptides (Fig. 5G, Table S5).

Finally, we conducted WGCNA on NK cells within the Twin-MS dataset to test whether *MS4A1* appears in any transcriptional module. We found that *MS4A1* is transcribed within the module distinguished by high GZMK expression, confirming higher expression of *MS4A1* in the $CD56^{bright}$-like cluster. *MS4A1* expression correlated positively with genes including *SELL*, *IL7R*, *GZMK*, *XCL1*, and *TCF7* (Fig. 5H, Table S6).

Next, we analyzed the COMBAT study dataset, a CITE-seq multi-omics dataset derived from the PBMC samples of COVID-19 patients.[12] This dataset contained 69,927 NK cells, 884 (1.26%) of which expressed *MS4A1*. Importantly, DGE analysis of cell surface proteins validated that CD20 protein expression is higher on *MS4A1*-expressing NK cells compared to other NK cells (Fig. 5I, Table S7). Moreover, CD56, CD27, CD62L, CD44, NKp46 (CD335), CD2, and CD11c were more abundant, while CD16, KLRG1, CD57, and CX3CR1 were less abundant on these cells, confirming our results obtained by flow cytometry analysis (Fig. 5I, Table S8). Additionally, *MS4A1* expressing cells were again more frequent in the $CD56^{bright}$ $CD16^{int}$ subcluster (3.15%), compared to the $CD16^{hi}$ cells (1.04%). DGE analysis gave a list of upregulated genes in *MS4A1* expressing NK cells, that highly overlap with the results of the Twin-MS dataset (Fig. 5J, Table S8).

The results so far show that $CD20^+$ NK cells are enriched in the $CD56^{bright}$ cell population, which is predominantly present in the tissues, especially secondary lymphoid organs, and underrepresented in blood.[13] Therefore, to get a more detailed picture of the *MS4A1*-expressing NK cells, we analyzed another scRNA-seq dataset that combines data from FACS-sorted $CD45^+CD56^+CD3^-CD14^-CD15^-CD163^-$ NK cells of paired blood and resected metastatic melanoma tissues obtained from 5 patients.[14] The *MS4A1*-expressing NK cell ratio was 0.35% (69/19,859) in blood, whereas it was much higher (4.21% [545/12,936]) in tumor tissue (Fig. 6A–C). The percentage of *MS4A1*-expressing NK cells was again highest among the $IL7R^+GZMK^+GZMB^{low}$ $CD56^{bright\text{-}like}$ cells (cluster 1 [6%]), followed by $IL7R^+GZMK^-GZMB^-$ NK

Downloaded from https://academic.oup.com/jimmunol/article/214/10/2585/8240403 by Koc University SK Library (KOC) user on 05 December 2025

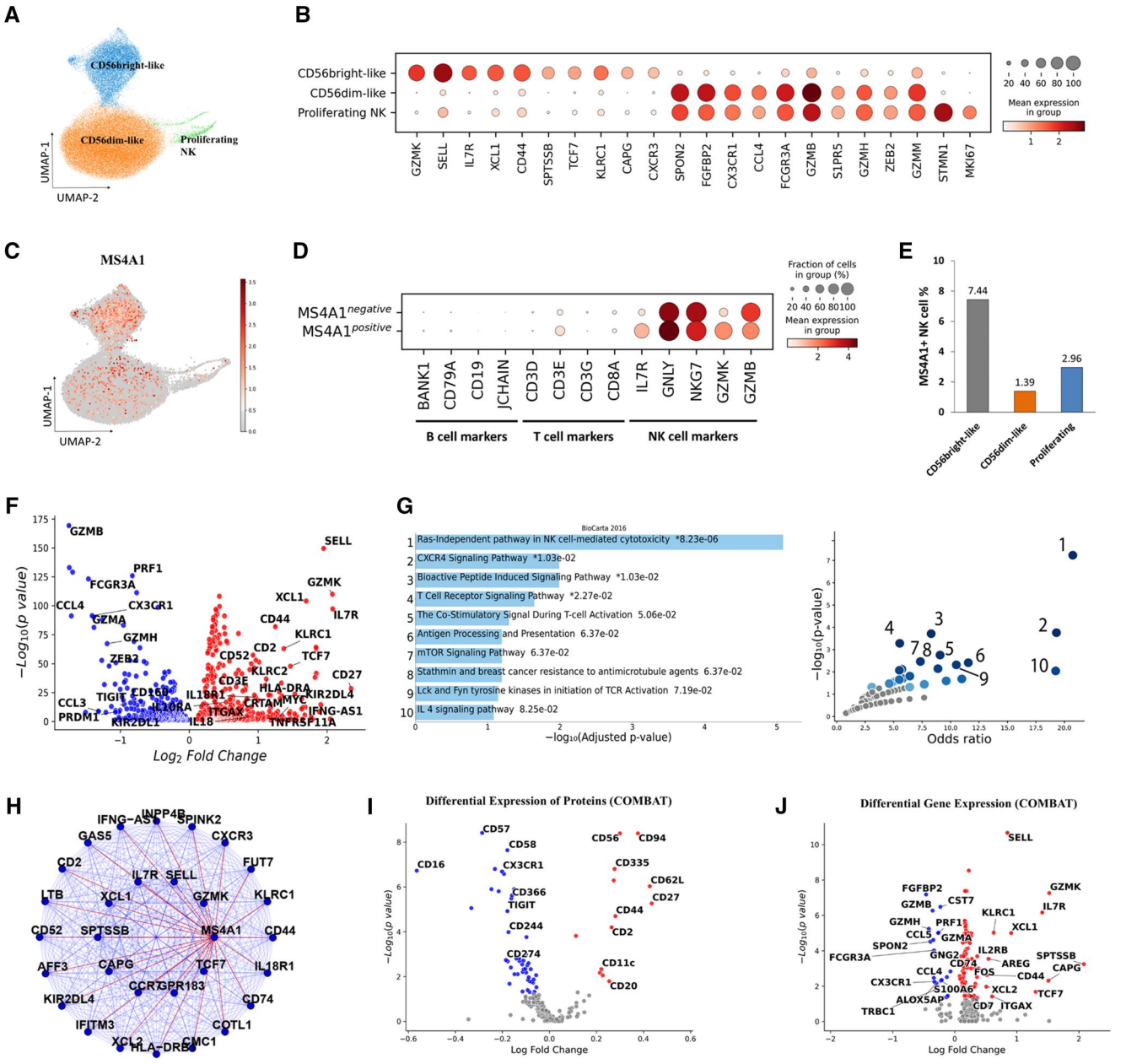

Figure 5. Molecular features of *MS4A1*-expressing NK cells in the Twin-MS dataset. (A) UMAP graph showing the identified NK cell subclusters. (B) Dot plot of the top differentially expressed genes in each subcluster. (C) UMAP plot demonstrating the distribution of *MS4A1*-expressing NK cells (red dots, enlarged for clarity). (D) Dot plot showing expression of marker genes for B cells, T cells, and NK cells demonstrates that there is no B- or T-cell contamination in the NK cell cluster. (E) *MS4A1*-expressing NK cells are enriched in the CD56$^{bright-like}$ subset. (F) Volcano plot demonstrating the differentially expressed genes in *MS4A1*-expressing NK cells vs others. (G) The pathways that are active in *MS4A1*-expressing NK cells revealed by GSEA of the upregulated genes by using the BioCarta 2016 database (left); graph showing the *P* value and odds ratio of each pathway (right). (H) The network of genes coexpressed with *MS4A1* in the CD56^{bright}-like module, as revealed by WGCNA. Lines connecting the dots represent connectivity between the genes. (I) Differential expression of cell surface proteins in MS4A1 expressing cells versus other NK cells in the CITE-seq multi-omics dataset of the COMBAT study. (J) Differential gene expression analysis of MS4A1 expressing NK cells compared to other NK cells in the same study.

precursor (NKP) cells (cluster 3 [3.4%]), *STMN1*$^{+}$ proliferating NK cells (cluster 4 [1.8%]), *IL7R*$^{-}$*GZMK*$^{+}$*GZMB*^{low}CD56^{int} cells (cluster 2 [1.15%]), and *IL7R*$^{-}$*GZMK*$^{-}$*GZMB*^{high}CD56$^{dim-like}$ cells (clusters 0 and 5 [0.06% and 0%, respectively]) (Fig. 6D–H). The DGE analysis of *MS4A1*-expressing NK cells yielded highly overlapping results with the Twin-MS and COVID-19 datasets in terms of upregulation of the CD56^{bright}-related genes and downregulation of the CD56^{dim}-related genes in both blood and tumor (Fig. S5A, B; Tables S9 and S10, respectively).

Next, to gain more insight into the molecular mechanisms behind the activated state of *MS4A1*$^{+}$ NK cells, we conducted a DGE analysis restricted to the cells in cluster 1, which includes 83% (511/614) of all *MS4A1*-expressing NK cells. This analysis yielded 561 upregulated and 51 downregulated genes in *MS4A1*-expressing *IL7R*$^{+}$ *GZMK*$^{+}$*GZMB*^{low}CD56$^{bright-like}$ cells (Fig. 6I, Table S11). Gene Ontology (GO) analysis of the upregulated genes, based on cellular components, indicated associations with focal adhesions, the nucleus, the actin cytoskeleton, and lipid rafts.

Downloaded from https://academic.oup.com/jimmunol/article/214/10/2585/8240403 by Koc University SK Library (KOC) user on 05 December 2025

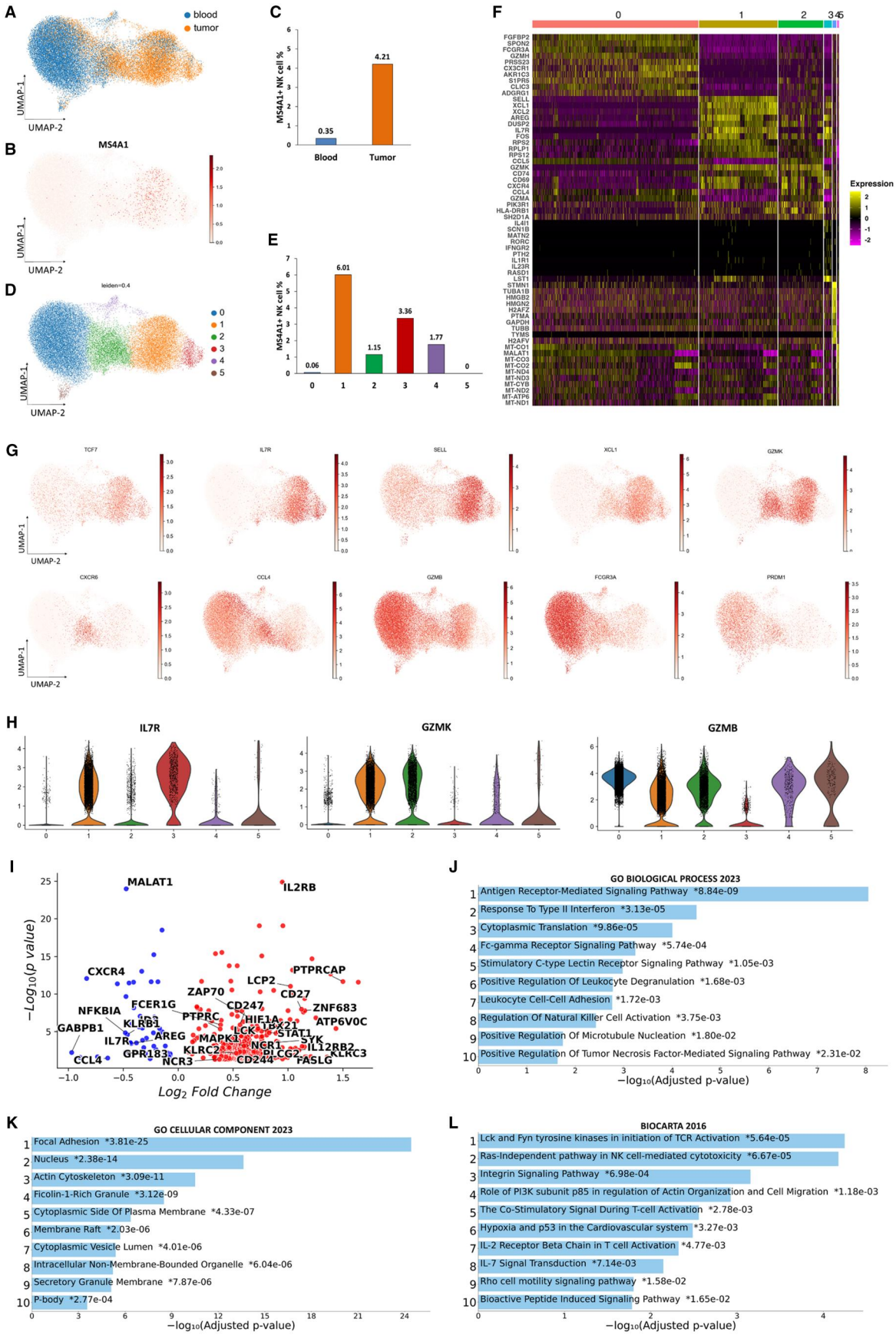

Figure 6. Distribution and molecular features of *MS4A1*-expressing NK cells in the paired blood and tumor samples from patients with melanoma. (A) UMAP plot shows that NK cells obtained from the blood and tumor tissues cluster in opposite sides and have little overlap. (B and C) *MS4A1* expression is scarce in blood NK cells whereas it is dramatically enriched in tumor tissues. (D) UMAP graph showing the major subclusters of NK cells (Leiden 0.3).

(Continued)

Downloaded from https://academic.oup.com/jimmunol/article/214/10/2585/8240403 by Koc University SK Library (KOC) user on 05 December 2025

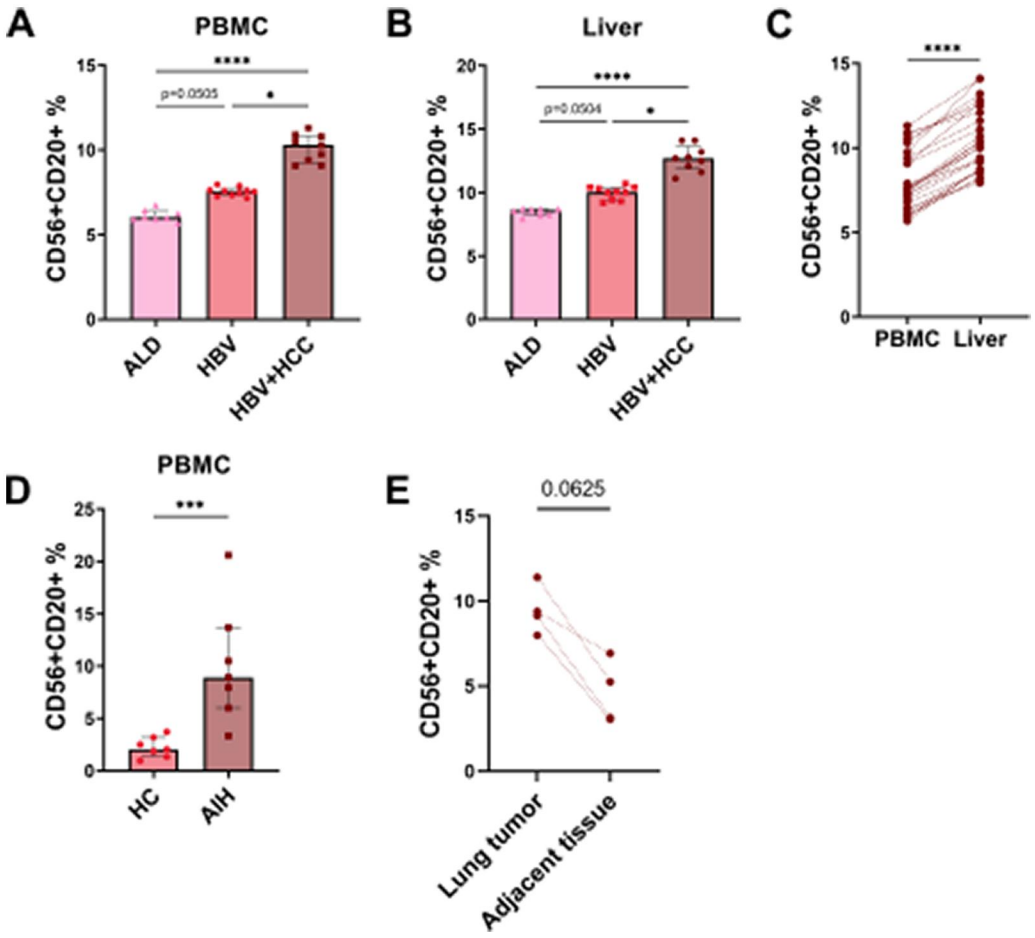

Figure 7. CD20+ NK cells are increased in the tissues of patients with inflammatory disorders. (A and B) CD56+CD20+ cells were expanded in the blood (A) and liver (B) tissues obtained from patients with HBV-related CLD and HCC (HBV+ HCC) ($n = 9$) compared to the patients only with chronic HBV ($n = 10$) infection. In addition, there was a strong tendency for CD56+CD20+ cell expansion in HBV-related CLD compared to alcoholic liver disease (ALD) ($n = 8$), again in both tissue types (A and B). *P* values were calculated using Kruskal–Wallis test with Dunn multiple comparisons post hoc correction. (C) CD56+CD20+ cells are enriched in the liver of patients with CLDs (ALD, HBV, and HBV+ HCC) compared to the paired peripheral blood ($n = 27$). (D) The ratio of CD56+CD20+ cells is increased in the blood of children with autoimmune hepatitis (AIH) (n = 7) compared to HCs (n = 7). (E) There was a tendency for the enrichment of CD56+CD20+ cells inside the lung tumor compared to the paired surrounding tissue ($n = 4$). *P* values were calculated using Wilcoxon matched-pairs signed-rank test. $*P < 0.05$, $**P < 0.01$, $***P < 0.001$, $****P < 0.0001$.

Analysis of biological processes revealed involvement in receptor-mediated signaling (C-type lectin receptor and Fc-γ receptor pathways), responses to type II IFN and TNF, leukocyte degranulation, NK cell activation, cell adhesion, protein translation, and microtubule nucleation (Fig. 6J, K; Fig. S5C, D; Tables S12 and S13). GSEA showed activation of the pathways related to receptor signaling through Lck and Fyn tyrosine kinases, Ras-independent NK cell–mediated toxicity (through NKG2C and NKG2E receptors), actin organization, cell migration, hypoxia response, and STAT1 signaling. (Fig. 6L, Fig. S5E, Table S14). Additionally, CD27, IL-12RB2, IL-2RB, TBX21, CD244, NCR1, NCR3, CD247, and FCER1G were also upregulated, highlighting the highly responsive status of CD20+ NK cells to IL-12, IL-15, and activating NK cell receptors, and the tendency of these cells to differentiate into a mature type 1 immune cell phenotype upon stimulation.

In summary, these results provide a comprehensive explanation for the molecular basis of the remarkably active cell state observed in CD20+ NK cells, as revealed by the flow cytometry experiments, despite their seemingly less mature phenotype.

CD56+CD20+ cells are expanded in inflammatory disorders, including chronic HBV infection, HCC, autoimmune hepatitis, and lung cancer

Our results so far indicate that CD56+CD20+ cells display features of memory-like NK cells. Therefore, we wondered whether expansion of CD56+CD20+ cells is seen in other

Figure 6. Continued
(E) *MS4A1* expression is highest in cluster 1, followed by clusters 3 and 4, whereas it is very low in clusters 0 and 5. (F) Heatmap demonstrating the highly expressed genes in each cluster. (G) Selected genes that are enriched in various clusters are highlighted in the UMAP plot. *TCF7*, *IL7R*, *SELL*, and *XCL1* are highly expressed in both cluster 1 (CD56bright-like) and 3 (NKP cluster), whereas *GZMK* is expressed by clusters 1 and 2 (CD56int), but not 3. *CXCR6* and highly expressed *CCL4* are enriched in cluster 2. *GZMB*, *FCGR3A*, and *PRDM1* are highly expressed by the CD56dim-like clusters 0 and 5. (H) Bar plots showing the gene expression level of marker genes *IL7R*, *GZMK*, and *GZMB* in different NK subclusters. (I) Volcano plot showing the DGEs in *MS4A1*-expressing NK cells of cluster 1 (CD56bright-like). (J and K) GO annotation analysis of the upregulated genes in *MS4A1*-expressing NK cells of cluster 1. (L) GSEA of *MS4A1*-expressing NK cells of cluster 1 according to the BioCarta 2016 database.

Downloaded from https://academic.oup.com/jimmunol/article/214/10/2585/8240403 by Koc University SK Library (KOC) user on 05 December 2025

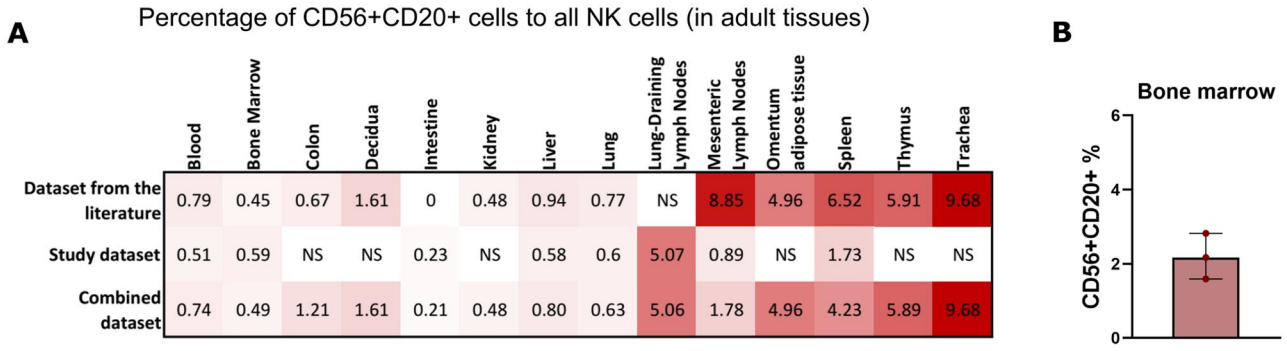

Figure 8. CD20$^+$ NK cells are abundant in secondary lymphoid organs, and present during development. (A) Heatmap showing the distribution of *MS4A1*-expressing NK cells in different organs in the cross-tissue immune cell analysis study, which was performed by the analysis of adult human tissues. Enrichment of these cells in the secondary lymphoid organs is evident. Numbers show the percentage of *MS4A1*-expressing NK cells in each organ. Data from tissues with <100 available cells are not shown (NS). (B) The presence of CD20$^+$ NK cells in the bone marrow was verified by flow cytometry in patients with leukemia and recent bone marrow transplantation.

inflammatory disorders. First, we analyzed paired peripheral blood and hepatic tissue from patients with alcohol-related liver disease and chronic HBV infection with or without HCC (Table S15). CD56$^+$CD20$^+$ cells were expanded in the blood and liver tissues obtained from patients with HBV-related HCC compared to the patients only with chronic HBV infection (Fig. 7A, B). Moreover, there was a tendency for CD56$^+$CD20$^+$ cell expansion in persistent HBV infection–related CLD compared to alcohol-related liver disease, again in both tissue types tested (Fig. 7A, B). In addition, CD56$^+$CD20$^+$ cells were enriched in the liver compared to the paired blood samples (Fig. 7C).

Next, we investigated children with autoimmune hepatitis and found that CD56$^+$CD20$^+$ cells are more frequent in the peripheral blood of patients compared to HCs (Fig. 7D, Table S15).

Last, we examined samples of surgically removed lung cancer tissue and neighboring healthy tissue. Again, there was a tendency for the enrichment of CD56$^+$CD20$^+$ cells in the cancer tissue compared to the neighboring tissue (Fig. 7E).

MS4A1-expressing NK cells are enriched in secondary lymphoid organs

Our results show that CD56$^+$CD20$^+$ cells carry a lymph node–homing capacity, characterized by high expression of *SELL*. Therefore, we investigated the distribution of CD56$^+$CD20$^+$ cells throughout the body in the publicly available human cross-tissue immune cell analysis dataset by Domínguez Conde et al.[15]

This is an adult tissue dataset and combines independent data from 2 sources: curated information from published studies and original data generated by the study team. First, we observed that *MS4A1* is expressed in a small fraction of NK cells in the bone marrow in both resources. Second, we observed that the ratio of *MS4A1*-expressing NK cells varied among tissues. The percentage was relatively lower in the peripheral blood, bone marrow, and most solid tissues, whereas it was higher in the secondary lymphoid organs, especially in the spleen. The rate of CD20 expression was highest among the CD56^{bright}-like NK cluster characterized by high *GZMK* and *SELL* expression, in line with our previous findings (Fig. 8A, Table S16). By using flow cytometry, we verified the presence of CD20$^+$ NK cells in the recently transplanted bone marrow obtained from patients with leukemia who were treated with immune suppression followed by bone marrow transplantation (Fig. 8B).

Discussion

Herein, we identified that a fraction of NK cells express CD20. These CD56$^+$CD20$^+$ cells have an active phenotype and superior functional capacity, in terms of cytotoxicity and cytokine secretion. Despite increased functionality, these cells are not terminally differentiated and carry homeostatic and memory-like features, evidenced by high *TCF7*, *IL7R*, and *CD27* expression and higher proliferative capacity. CD56$^+$CD20$^+$ cells are preferentially located in secondary lymphoid organs and are expanded in the blood and disease-relevant tissues in inflammatory disorders.

The features of CD20$^+$ NK cells identified in this study exhibit similarities to CD20$^+$ T cells. CD3$^+$CD20$^+$ cells are recognized as proinflammatory cells, characterized by an activated phenotype and increased cytokine secretion upon stimulation.[4,5,8] Likewise, our findings indicate an elevated proportion of CD20$^+$ NK cells expressing the activation markers CD69 and CD137, along with the activating receptor NKp46. Additionally, we observed heightened production and secretion of TNF-α, IFN-γ, GM-CSF, and IL-10 after stimulation in CD56$^+$CD20$^+$ cells. Phenotypically, CD3$^+$CD20$^+$ cells are predominantly enriched in Th1 and Tc1 memory subsets, exhibiting lower abundance among naïve and terminal effector subsets.[5] Similarly, we observed a diminished proportion of CD56$^+$CD20$^+$ cells expressing markers associated with mature and terminally differentiated NK cells, such as CD57, CD16, GzmB, and perforin. A striking feature of CD20$^+$ NK cells is their heightened cytotoxic activity. While previous research has shown that CD3$^+$CD20$^+$ cells are enriched for CD8$^+$ cytotoxic T cells, it remains uncertain whether these cells also exhibit elevated cytotoxicity, necessitating further investigation in future studies.

Our investigation revealed a higher percentage of CD20 expression among CD56^{bright} cells as compared to CD56^{dim} NK cells. CD56^{bright} NK cells are known for their potent cytokine-producing abilities with restricted cytotoxicity. However, we found that CD20$^+$ NK cells exhibit greater cytotoxicity and efficiency in killing K562 cells. Several findings reveal the cellular mechanisms behind the superior cytolytic potential of CD56$^+$CD20$^+$ cells. First, CD56$^+$CD20$^+$ cells exhibit enhanced degranulation, with higher granule secretion per cell and increased expression of cytotoxic molecules compared to CD20$^-$ cells. Second, CD56$^+$CD20$^+$ cells display elevated levels of apoptosis-inducing receptors FASL and TRAIL on their surface. Collectively, these features underscore the enriched cytotoxic arsenal of CD20$^+$ NK cells,

Downloaded from https://academic.oup.com/jimmunol/article/214/10/2585/8240403 by Koc University SK Library (KOC) user on 05 December 2025

coupled with an efficient molecular machinery facilitating effective lytic granule release. These observations strongly indicate a primed state in these cells, poised for robust type 1 immune responses.

Analysis of publicly available scRNA-seq data unveiled the molecular basis underlying this heightened polyfunctionality. We observed upregulation of ITAM-bearing NK receptor complexes *CD247* (CD3ζ) and *FCER1G* (FcεRI-γ), along with members of Src family kinases (*LCK*, *LYN*, *FYN*, *FGR*), tyrosine kinases (*SYK* and *ZAP70*), *PLCG2*, *LCP2*, and several actin cytoskeleton and membrane raft–related molecules like *ZYX*, *LCP1*, *ACTB*, and *RFTN1*, among others, in *MS4A1*-expressing NK cells. Additionally, genes associated with cytolytic granule formation and microtubule organization were also found to be upregulated in *MS4A1*-expressing NK cells. These findings suggest that CD20 may interact with NK cell–activating receptors, leading to an amplification of stimulatory signals upon stimulation. This, in turn, may trigger protein synthesis and cytoskeleton reorganization, ultimately culminating in increased cytokine and cytotoxic granule release. Identification of the specific protein–protein interactions will require further studies.

We found that expression of *MS4A1* correlates with several other genes including *TCF7*, *GZMK*, *SELL*, *IL7R*, and *XCL1*. *TCF7* codes for the transcription factor Tcf1 that plays a critical role in NK cell survival during maturation and upon activation by limiting excessive GzmB expression.[16] GzmK is known for its prominent proinflammatory function and its role in endothelial activation and breaking of the blood–brain barrier.[17] Recently, GrK-expressing CD8$^+$ T cells have been described as tissue-enriched cells and reported to constitute the core inflammatory population in tissues undergoing inflammation.[18] We observed a dramatic upregulation of GrK in CD20$^+$ NK cells after incubation with IL-2, IL-15, and K562 cells. Thus, GrK expression may be a significant contributor of the tissue-enriched and proinflammatory nature of CD56$^+$CD20$^+$ cells.

Molecules previously linked to enhanced functionality and memory-like features in NK cells are similarly upregulated in CD20$^+$ NK cells. Among these, *SELL* encodes for CD62L. CD62L$^+$CD56^{dim} NK cells were previously reported to be polyfunctional cells with a higher killing and cytokine production capacity and preserve their ability to proliferate during viral infection.[19] *CD44* has a role in cytoskeleton rearrangement and raft reorganization, and signaling through CD44 has been shown to enhance NK cell cytotoxic function. CD2 is important for NK cell immune synapse formation and recruits CD16 to the immune synapse, lowering the threshold for activation. It is upregulated in adaptive NK cells even in the absence of NKG2C.[20] Finally, *CD52* was reported among the top upregulated genes together with *KLRC2*, *CD2*, and *CD3E* in the adaptive NK cell population in cytomegalovirus-seropositive patients in 2 recent studies.[21,22] Another memory-like feature of CD56$^+$CD20$^+$ cells is their higher proliferative capacity in response to IL-2 and IL-15 stimulation.

Our investigation encompassing 2 distinct cohorts of individuals affected by neurological and hepatic disorders revealed an expansion of CD56$^+$CD20$^+$ cells in both the blood and disease-relevant tissues. Remarkably, the degree of expansion was more pronounced in MS compared to ONDs, and it was also higher in individuals with HBV-related HCC compared to those with chronic HBV-related CLD. Additionally, we observed a strong correlation between CD20$^+$ NK cells and CD20$^+$ T cells and B cells in pwMS, highlighting the relevance to these cells in adaptive immune response. Taken together, these clinical findings, along with the molecular insights provided above, suggest that elevated CD20 expression may be a common mechanism in various lymphocyte subtypes during chronic inflammatory conditions and is associated with enhanced functionality and memory features.

There are some limitations of our study. First, while our flow cytometry and functional assays identified distinctive features of CD20$^+$ NK cells, these findings were primarily based on in vitro assays, which may not fully capture the in vivo behavior of these cells in complex tissue environments. Second, although we analyzed publicly available scRNA-seq datasets to validate our findings, the limited availability of high-resolution datasets from diverse patient populations may restrict the generalizability of our results across different inflammatory and oncologic conditions. Third, while we observed an enrichment of CD20$^+$ NK cells in inflamed tissues and peripheral blood of patients with various inflammatory diseases, the underlying mechanisms driving their expansion and precise role in disease progression remain to be fully elucidated. Finally, our study did not address the long-term stability and functional plasticity of CD20$^+$ NK cells, which may be relevant for understanding their potential as therapeutic targets. Future studies should aim to address these limitations by examining CD20$^+$ NK cells in more diverse patient cohorts and exploring their in vivo functions in disease models.

In conclusion, we have identified that CD20 expression is not restricted to B cells, and T cells and NK cells can also express CD20. These CD56$^+$CD20$^+$ NK cells exhibit enhanced cytokine production, cytotoxicity, and proliferative capacity, and are expanded in various inflammatory disorders. The unique features of CD56$^+$CD20$^+$ cells render them both as possible treatment targets and as therapeutic tools. Further investigations are warranted to investigate the role of CD56$^+$CD20$^+$ cells in various disorders.

Acknowledgments

We would like to thank to the patients and healthy volunteers who participated in this research project. We are also thankful to Prof. Dr Caner Süsal and Dr Miriam Fichtner for reviewing the first draft of our manuscript and their invaluable comments. The authors gratefully acknowledge the use of the services and facilities of the Koç University Research Center for Translational Medicine, funded by the Presidency of Turkey, Presidency of Strategy and Budget. During the preparation of this work the authors used ChatGPT 3.5 for English-language editing of this article. After using this tool, the authors reviewed and edited the content as needed and take full responsibility for the content of the publication.

Author contributions

Özgür Albayrak (Data curation [lead], Formal analysis [lead], Funding acquisition [supporting], Investigation [lead], Methodology [lead], Project administration [lead], Visualization [equal], Writing—original draft [equal]), Ergün Tiryaki (Formal analysis [equal], Investigation [equal], Visualization [equal], Writing—original draft [equal]), Nazan Akkaya (Investigation [supporting], Resources [supporting]), Ali Burak Kizilirmak (Investigation [supporting], Resources [supporting]), Tansu Doran (Resources [supporting]), Gökçe Gökmenoglu (Resources [supporting]), Muhammed Yüksel (Resources

Downloaded from https://academic.oup.com/jimmunol/article/214/10/2585/8240403 by Koc University SK Library (KOC) user on 05 December 2025

[supporting]), Bürge Ulukan (Resources [supporting]), Mina Üzülmez (Resources [supporting]), Isil Baytekin (Resources [supporting]), Önder Kemal Soylu (Resources [supporting]), Günes Esendagli (Resources [supporting], Writing—review & editing [equal]), Ingrid Meinl (Resources [supporting]), Mesrure Köseoglu (Resources [supporting]), Burcu Yüksel (Resources [supporting]), Suat Erus (Resources [supporting]), Çigdem Arikan (Resources [supporting]), Seçil Vural (Writing—review & editing [equal]), Müjdat Zeybel (Resources [supporting], Writing—review & editing [equal]), Aysun Soysal (Resources [lead]), Edgar Meinl (Writing—review & editing [equal]), and Atay Vural (Conceptualization [lead], Data curation [equal], Formal analysis [equal], Funding acquisition [lead], Investigation [equal], Project administration [lead], Supervision [lead], Visualization [lead], Writing—original draft [lead])

Supplementary material

Supplementary material is available at *The Journal of Immunology* online.

Funding

This study was funded by TÜBİTAK (grant numbers 118S397 and 220S638) and an Alexander von Humboldt Foundation Return Fellowship. O.A. was supported by the Multiple Sclerosis International Federation Du Pré Grant.

Conflicts of interest

E.M. received honoraria from Merck, Roche, Novartis, and TEVA and grant support from Novartis, Roche, Merck, GlycoEra, Alexion, and Horizon. Other authors declare that they have no competing interests.

Data availability

All data are available in the main text or the supplementary materials.

References

1. Baker D, Marta M, Pryce G, Giovannoni G, Schmierer K. Memory B cells are major targets for effective immunotherapy in relapsing multiple sclerosis. EBioMedicine. 2017;16:41–50.
2. Furman MJ et al. B cell targeted therapies in inflammatory autoimmune disease of the central nervous system. Front Immunol. 2023;14:1129906.
3. Hultin LE, Hausner MA, Hultin PM, Giorgi JV. CD20 (pan-B cell) antigen is expressed at a low level on a subpopulation of human T lymphocytes. Cytometry. 1993;14:196–204.
4. Schuh E et al. Features of human $CD3^{+}CD20^{+}$ T cells. J Immunol. 2016;197:1111–1117.
5. von Essen MR et al. Proinflammatory $CD20^{+}$ T cells in the pathogenesis of multiple sclerosis. Brain. 2019;142:120–132.
6. Wilk E et al. Depletion of functionally active $CD20^{+}$ T cells by rituximab treatment. Arthritis Rheum. 2009;60:3563–3571.
7. Palanichamy A et al. Rituximab efficiently depletes increased CD20-expressing T cells in multiple sclerosis patients. J Immunol. 2014;193:580–586.
8. Ochs J et al. Proinflammatory CD20(+) T cells contribute to CNS-directed autoimmunity. Sci Transl Med. 2022;14:eabi4632.
9. Chen Q, Yuan S, Sun H, Peng L. CD3(+)CD20(+) T cells and their roles in human diseases. Hum Immunol. 2019;80:191–194.
10. Mudd TW, Jr., Lu C, Klement JD, Liu K. MS4A1 expression and function in T cells in the colorectal cancer tumor microenvironment. Cell Immunol. 2021;360:104260.
11. Ingelfinger F et al. Twin study reveals non-heritable immune perturbations in multiple sclerosis. Nature. 2022;603:152–158.
12. COvid-19 Multi-omics Blood ATlas (COMBAT) Consortium. A blood atlas of COVID-19 defines hallmarks of disease severity and specificity. Cell. 2022;185:916–938 e958.
13. Melsen JE, Lugthart G, Lankester AC, Schilham MW. Human circulating and tissue-resident CD56(bright) natural killer cell populations. Front Immunol. 2016;7:262.
14. de Andrade LF et al. Discovery of specialized NK cell populations infiltrating human melanoma metastases. JCI Insight. 2019;4:e133103.
15. Domínguez Conde C et al. Cross-tissue immune cell analysis reveals tissue-specific features in humans. Science. 2022;376:eabl5197.
16. Jeevan-Raj B et al. The transcription factor Tcf1 contributes to normal NK cell development and function by limiting the expression of granzymes. Cell Rep. 2017;20:613–626.
17. Herich S et al. Human $CCR5^{high}$ effector memory cells perform CNS parenchymal immune surveillance via GZMK-mediated transendothelial diapedesis. Brain. 2019;142:3411–3427.
18. Jonsson AH et al.; Accelerating Medicines Partnership RA/SLE Network. Granzyme K(+) CD8 T cells form a core population in inflamed human tissue. Sci Transl Med. 2022;14:eabo0686.
19. Juelke K et al. CD62L expression identifies a unique subset of polyfunctional CD56dim NK cells. Blood. 2010;116:1299–1307.
20. Liu LL et al. Critical role of CD2 co-stimulation in adaptive natural killer cell responses revealed in NKG2C-deficient humans. Cell Rep. 2016;15:1088–1099.
21. Ruckert T, Lareau CA, Mashreghi MF, Ludwig LS, Romagnani C. Clonal expansion and epigenetic inheritance of long-lasting NK cell memory. Nat Immunol. 2022;23:1551–1563.
22. Yang C et al. Heterogeneity of human bone marrow and blood natural killer cells defined by single-cell transcriptome. Nat Commun. 2019;10:3931.
23. Wolock SL, Lopez R, Klein AM. Scrublet: computational identification of cell doublets in single-cell transcriptomic data. Cell Syst. 2019;8:281–291 e289.
24. Korsunsky I et al. Fast, sensitive and accurate integration of single-cell data with Harmony. Nat Methods. 2019;16:1289–1296.
25. Traag VA, Waltman L, van Eck NJ. From Louvain to Leiden: guaranteeing well-connected communities. Sci Rep. 2019;9:5233.
26. Rezaie N, Reese F, Mortazavi A. PyWGCNA: a python package for weighted gene co-expression network analysis. Bioinformatics. 2023;39:btad415.
27. Csardi G, Nepusz T. The igraph software package for complex network research. *InterJournal, Complex Syst*. 2006;1695:1–9.
28. Xie Z et al. Gene set knowledge discovery with enrichr. Curr Protoc. 2021;1:e90.

© The Author(s) 2025. Published by Oxford University Press on behalf of The American Association of Immunologists.
This is an Open Access article distributed under the terms of the Creative Commons Attribution-NonCommercial License (https://creativecommons.org/licenses/by-nc/4.0/), which permits non-commercial re-use, distribution, and reproduction in any medium, provided the original work is properly cited. For commercial re-use, please contact reprints@oup.com for reprints and translation rights for reprints. All other permissions can be obtained through our RightsLink service via the Permissions link on the article page on our site—for further information please contact journals.permissions@oup.com.
The Journal of Immunology, 2025, 214, 2585–2599
https://doi.org/10.1093/jimmun/vkaf205
Research Article

Downloaded from https://academic.oup.com/jimmunol/article/214/10/2585/8240403 by Koc University SK Library (KOC) user on 05 December 2025